Neurosurgical Review (2019) 42:867–876
https://doi.org/10.1007/s10143-018-01061-5

ORIGINAL PAPER

Predictive markers for *MGMT* promoter methylation in glioblastomas

Tokunori Kanazawa[1] · Yasuhiro Minami[2] · Masahiro Jinzaki[2] · Masahiro Toda[1] · Kazunari Yoshida[1] · Hikaru Sasaki[1]

Received: 1 July 2018 / Revised: 23 October 2018 / Accepted: 22 November 2018 / Published online: 23 January 2019

Abstract

The promoter methylation status of the *O*^{6}*-methylguanine-DNA methyltransferase* (*MGMT*) gene has been described as the most important predictor of chemotherapeutic response and patients' survival in glioblastomas (GBs). Therefore, prediction of the *MGMT* promoter methylation status by imaging would help to preoperatively decide the overall treatment strategy as well as surgical strategy. This study aimed to detect imaging parameters to predict *MGMT* promoter methylation in GBs by using a commercially available software. We investigated three imaging features (ring enhancement, tumor location, and laterality) and apparent diffusion coefficient (ADC) parameters in 48 newly diagnosed GBs treated at Keio University Hospital in 2006 or later. For ADC, texture analyses were performed. Regions of interest (ROIs) were drawn manually with reference to contrast-enhanced areas, excluding necrotic and cystic regions. Mean ADC value and ADC histogram parameters, including kurtosis, skewness, and entropy, were compared with *MGMT* promoter methylation. Each parameter was evaluated to determine correlation with *MGMT* promoter methylation, and the parameters with significant associations with the methylation status were correlated with the *MGMT*-positive cell ratio determined by immunohistochemistry (IHC) analysis. The mean ADC value and ADC entropy were significantly associated with *MGMT* promoter methylation. The combination of mean ADC value and ADC entropy predicted *MGMT* promoter methylation, with a PPV of 81.2% and specificity of 88.9%. The mean ADC value and ADC entropy were negatively correlated with the *MGMT*-positive cell ratio in the IHC analysis. This study demonstrated that texture analyses of ADC histograms in GBs were predictive of *MGMT* promoter methylation.

Keywords Glioblastoma · Texture analysis · ADC · *MGMT*

Introduction

Glioblastoma (GB) is one of the most common malignant primary brain tumors [32, 33]. Despite multidisciplinary treatments, the median overall survival (OS) ranges from 10 to 20 months [38, 42, 43]. The most important predictive marker for chemotherapeutic response and survival of patients with GBs is the promoter methylation status of the *O*^{6}*-methylguanine-DNA methyltransferase* (*MGMT*) gene [12, 18, 19], which is the key enzyme in DNA repair and counteracts the genotoxic effects of alkylating agents [36, 47]. The presence of *MGMT* promoter methylation is associated with low levels of *MGMT* proteins, which consequently leads to reduction in DNA repair activity against alkylating agents. However, molecular information is informed only after invasive surgical resection. If the *MGMT* promoter methylation status is informed by imaging before initial surgery, such information would be useful for the overall treatment strategy as well as surgical strategy, including placement of BCNU wafers.

To date, it has been reported that certain magnetic resonance imaging (MRI) features, such as ring enhancement and tumor laterality, correlated with *MGMT* promoter methylation status [7, 9, 10]. Apparent diffusion coefficient (ADC) also has been used as a potential predictor of *MGMT* promoter methylation, but without expert consensus [5, 16, 17, 31, 34, 37, 44]. Recently, researchers drew attention to quantitative methods, often with image texture analysis and machine-learning algorithms, but these time-consuming methods were unsuitable for daily clinical use.

Electronic supplementary material The online version of this article (https://doi.org/10.1007/s10143-018-01061-5) contains supplementary material, which is available to authorized users.

✉ Tokunori Kanazawa
norinori0128jp@yahoo.co.jp

[1] Department of Neurosurgery, Keio University School of Medicine, 35 Shinanomachi, Shinjuku-ku, Tokyo 160-8582, Japan

[2] Department of Diagnostic Radiology, Keio University School of Medicine, 35 Shinanomachi, Shinjuku-ku, Tokyo 160-8582, Japan

Therefore, the aim of the present study was to identify imaging parameters to predict *MGMT* promoter methylation in GBs by using commercially available software and routine imaging data. We determined if there were significant associations between *MGMT* promoter methylation status and imaging parameters. The imaging parameters significantly associated with *MGMT* promoter methylation were subjected to correlation analysis to quantitatively assess any associations with the *MGMT*-positive cell ratio in immunohistochemistry (IHC) analysis. Finally, we also determined if any of the imaging parameters correlated with clinical outcomes of GB patients.

Materials and methods

Clinical samples

Pathological and clinical records and imaging data of patients treated at the Department of Neurosurgery, Keio University Hospital between March 2006 and October 2017 were reviewed. The following inclusion criteria were used: (a) newly diagnosed, untreated GB of World Health Organization (WHO) grade IV [24, 25, 28, 29]; and (b) patients who underwent preoperative MRI, including diffusion-weighted imaging (DWI; $b = 0$ s/mm^2 and $b = 1000$ s/mm^2). Accordingly, we recruited 48 patients with newly diagnosed and pathologically confirmed GB. This study was approved by the Institutional Review Board of Keio University. Written informed consent was obtained from all patients included in this study.

Assessment of *MGMT* promoter methylation status

Tumor DNA was isolated from formalin-fixed paraffin-embedded section. The methylation status of the *MGMT* promoter was assessed by methylation-specific polymerase chain reaction (PCR) using the EZ DNA Methylation-Direct kit (Zymo Research Corp., Orange, CA, USA) as previously described [30, 40].

Then, we quantitatively evaluated the methylation ratio by IHC of *MGMT* because it was a fast and less expensive method. *MGMT* IHC was performed with mouse monoclonal anti-*MGMT* antibody (MT 3.1; 1:100; Thermo Scientific, Waltham, MA, USA) and an ImmPRESS Reagent kit (Vector Laboratories, Burlingame, CA, USA) after antigen retrieval for 20 min in a citrate buffer (pH 6). Normal brain was used as a positive control, and a previously proven *MGMT*-methylated GB was used as a negative control. The positive cell ratio of *MGMT* was determined by counting > 1000 tumor cells from > 3 HPFs (×200) showing the representative appearance of each tumor. Histiocytes and endothelial cells were excluded from the count as previously described [20].

Image acquisition

Preoperative MR (contrast-enhanced T1 and DWI) images were used for this study. All MR images were acquired by using a 1.5-T MRI scanner (Signa HDx or Optima MR 450 w; GE Healthcare, Waukesha, WI, USA) or a 3-T MRI scanner (SIGNA Pioneer or Discovery MR 750w Plus; GE Healthcare, Waukesha, WI, USA). Contrast-enhanced T1-weighted spin-echo (SE) images (repetition time (TR)/echo time (TE)/flip angle (FA), 560/9/90; field of view (FOV), 200 × 200 mm; section thickness, 5 mm at 1.5 T; TR/TE/FA, 600/12/90; FOV, 200 × 200 mm; section thickness, 5 mm at 3 T) were acquired in the axial and coronal planes after intravenous administration of 0.1 mmol/kg gadolinium-based contrast media (Omniscan: Daiichi Sankyo Co. Ltd., Tokyo, Japan, or Magnevist: Bayer Healthcare, Osaka, Japan, before 2015 and Gadovist: Bayer HealthCare, Osaka, Japan, or ProHance: Bracco Eisai Co. Ltd., Tokyo, Japan, after 2016).

DWI was obtained in the axial plane according to the following parameters (b values, 0 and 1000 s/mm^2; TR/TE, 5000/80; FOV, 200 × 200 mm; section thickness, 5 mm at 1.5 T; b values, 0 and 1000 s/mm^2; TR/TE, 5000/86; FOV, 250 × 250 mm; section thickness, 5 mm at 3 T).

Image data processing and image analysis (qualitative and quantitative image analysis)

First, as qualitative image analysis, the following three imaging characteristics were assessed on the basis of previous reports [7, 9, 10]: (a) ring enhancement of the majority of tumor signals on contrast-enhanced T1-weighted images, ring versus other; (b) tumor location, temporal location versus nontemporal location versus callosal location; and (c) tumor laterality, right versus left versus bilateral (Fig. 1). In case of mixed features (e.g., a ring-enhancing tumor with nodular enhancement or a left temporal tumor reaching the frontal lobe), the predominant imaging feature was selected. Two of the authors (HS and TK who have 28 and 8 years of experience, respectively, in neurosurgery and neuroimaging) who were blinded to the *MGMT* methylation status of the tumors independently assessed these features, and the final judgment was made by consensus of these evaluators for each imaging characteristic.

Then, as quantitative image analysis, texture analyses were performed. All DW MR images were transferred to a commercially available analysis software (Synapse Vincent Fujifilm, Tokyo, Japan). Using the DW MR images and the software, we calculated ADC maps. Regions of interest (ROIs) were drawn manually on the three representative slices. Tumor boundaries were defined with reference to the relatively higher signal on contrast-enhanced T1-weighted

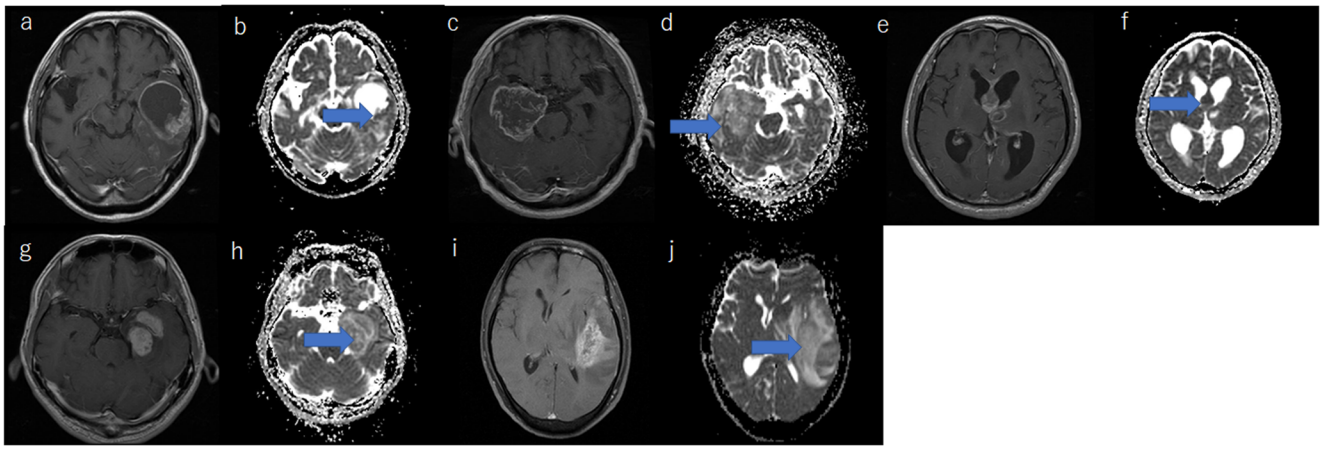

Fig. 1 MR images of representative cases. The arrows show contrast-enhanced areas on ADC maps and ROI segmentation was determined with reference to these areas. **a**, **b** Contrast-enhanced T1-weighted and ADC map images of a 79-year-old man with a left temporal tumor. This tumor was characterized by ring enhancement: ring, tumor location: temporal, and tumor laterality: left. (This ring-enhancing tumor with nodular enhancement was judged as ring because ring enhancement was predominant.) The promoter region of the *MGMT* gene was unmethylated. The mean ADC value is 1.00, and the mean ADC entropy is 6.123. **c**, **d** Contrast-enhanced T1-weighted and ADC map images of a 73-year-old man with a right temporal tumor. This tumor was characterized by ring enhancement: ring, tumor location: temporal, and tumor laterality: right. The promoter region of the *MGMT* gene was unmethylated. The mean ADC value is 1.05, and the mean ADC entropy is 6.231. **e**, **f** Contrast-enhanced T1-weighted and ADC map images of a 48-year-old man with a corpus callosal tumor. This tumor was characterized by ring enhancement: other, tumor location: callosal, and tumor laterality: bilateral. The promoter region of the *MGMT* gene was unmethylated. The mean ADC value is 0.94, and the mean ADC entropy is 5.982. **g**, **h** Contrast-enhanced T1-weighted and ADC map images of a 41-year-old man with a left temporal tumor. This tumor was characterized by ring enhancement: other, tumor location: temporal, and tumor laterality: left. The promoter region of the *MGMT* gene was methylated. The mean ADC value is 1.38, and the mean ADC entropy is 6.245. **i**, **j** Contrast-enhanced T1-weighted and ADC map images of a 51-year-old man with a left temporal tumor. This tumor was characterized by ring enhancement: other, tumor location: temporal, and tumor laterality: left. The promoter region of the *MGMT* gene was methylated. The mean ADC value is 1.29, and the mean ADC entropy is 6.028

images and assessed independently by a single neurosurgeon (TK) and a single neuroradiologist (YM, with 8 years of experience in neuroimaging). Necrotic and cystic regions were excluded as previously reported [5, 17, 31, 34, 37, 44]. ADC histograms were generated with a bin of 1×10^{-5} mm^2/s and a range of 10×10^{-5} to 500×10^{-5} mm^2/s. The mean ADC value and ADC histogram parameters indicating kurtosis, skewness, and entropy were assessed from ROIs overlaid on the ADC maps and calculated by the average of the two evaluators.

Statistical analysis

To compare mean differences between the two groups (*MGMT*-methylated and *MGMT*-unmethylated groups), the unpaired Student's *t* test was used for continuous variables, and the Fisher's exact and χ^2 tests were used for categorical variables. A cutoff value was determined by receiver-operating characteristic (ROC) analysis. The predictive values of statistically significant imaging parameters, including sensitivity, specificity, positive predictive value (PPV), and negative predictive value (NPV), were calculated for *MGMT* promoter methylation. The significance of associations between *MGMT* promoter methylation and the imaging parameters were evaluated in univariate analysis by Fisher's exact test and the χ^2 test. Multivariate analysis was not applied considering the number of outcomes and variables. Then, the imaging parameters significantly associated with *MGMT* promoter methylation were subjected to correlation analysis using a Pearson linear regression model to determine if any parameters correlated with the *MGMT*-positive cell ratio in IHC analysis. Finally, survival analysis was performed by using the Kaplan–Meier method, and the associations of the imaging parameters with progression-free survival (PFS) and OS were compared by using the log-rank test. PFS and OS were calculated from the date of the first operation. Patients lost to follow-up were censored at the date they were last known to be free from tumor progression or patient death.

All statistical analyses were performed by using IBM SPSS Statistics 23.0 software. p values < 0.05 were considered as indicative of statistical significance. Multiple comparisons were accounted for by using a false discovery rate (FDR) adjustment at the $\alpha = 0.05$ level. FDR was considered more appropriate than other conservative corrections, such as Bonferonni, as a large number of associations were under investigation in this study [13].

Interobserver agreement for qualitative image analysis (assessment of ring enhancement) was calculated using the kappa statistic, because evaluations of tumor location and laterality were the same and reproducible between the two evaluators; $0 \leq \kappa \leq 0.2$ indicated slight agreement, $0.2 < \kappa \leq 0.4$ indicated fair agreement, $0.4 < \kappa \leq 0.6$ indicated moderate agreement, and $\kappa > 0.6$ indicated substantial agreement.

Results

The genetic and pathological characteristics of 48 GB patients of WHO grade IV based on the original institutional diagnoses are summarized in Table 1 [24, 25, 28, 29]. These patient populations comprised 31 men and 17 women, with a mean age of 60.1 years at the time of surgery (range, 25–85 years). According to the methylation status of the *MGMT* promoter by methylation-specific PCR, 21 (43.8%) patients were methylated and 27 (56.2%) were unmethylated. Twenty-eight of the 48 patients were examined by using 3 T MRI, and the other 20 were assessed by using 1.5 T MRI.

Image analysis and *MGMT* methylation status

Interobserver agreement measurement for ring enhancement was good ($\kappa = 0.864$ (0.788–0.940)). The qualitative image features of the 48 GB patients are summarized in Table 1. There were no significant differences in any of the imaging features between the *MGMT*-methylated and *MGMT*-unmethylated groups (Table 2).

From the texture analysis results, the mean ADC values and each ADC parameter were calculated (Table S1). The mean differences in each parameter between patients with and without *MGMT* promoter methylation were tested using the unpaired Student's *t* test. The mean ADC value and ADC entropy were significantly different between these patients (mean ADC value, $p = 0.002$; ADC entropy, $p = 0.013$, Table 2). Other textural parameters were not significantly different between the two groups (Table 2). A total of seven correlations were performed. After FDR correction, two significant associations ($p < 0.05$) were still statistically significant (italicized in Table 2).

Mean ADC value and ADC entropy as predictive markers for *MGMT* methylation status

The mean ADC value and ADC entropy were compared with *MGMT* methylation status. The predictive values of these parameters, including sensitivity, specificity, PPV, and NPV, were calculated for *MGMT* methylation status. The significance of associations between *MGMT* promoter methylation and these two parameters were evaluated by Fisher's exact test and the χ^2 test. The mean ADC cutoff value was determined and set at 1.12 according to ROC curve analysis ($p = 0.002$, AUC = 0.764 (95% confidence interval 0.623–0.904), Fig. S2). Mean ADC values ≥ 1.12 predicted *MGMT* methylation status, with a PPV of 70.8%, specificity of 74.1%, and sensitivity of 81.0% ($p = 0.000$, Table 3). Similarly, the ADC entropy cutoff value was calculated and set at 6.243 ($p = 0.009$, AUC = 0.721 (95% confidence interval 0.574–0.869), Fig. S3). ADC entropy ≥ 6.243 predicted *MGMT* methylation status, with a PPV of 68.2%, specificity of 74.1%, and sensitivity of 71.4% ($p = 0.002$, Table 3). The combination of mean ADC value and ADC entropy predicted *MGMT* methylation status, with a PPV of 81.2%, specificity of 88.9%, and sensitivity of 61.9% ($p = 0.000$, Table 3).

Negative correlation between ADC parameters and *MGMT*-positive cell ratio in IHC

The mean ADC value and ADC entropy were correlated with the *MGMT*-positive cell ratio in IHC to quantitatively assess the association between these parameters and *MGMT* promoter methylation ratio using a Pearson linear regression model. These two parameters revealed a negative correlation with the *MGMT*-positive cell ratio in IHC (mean ADC value, $R^2 = 0.153$, $p = 0.006$; ADC entropy, $R^2 = 0.78$, $p = 0.054$, Fig. 2).

Progression-free and overall survival

Finally, we determined if the mean ADC value and ADC entropy might be correlated with the clinical outcomes of GB patients by using the log-rank test. *MGMT*-methylated patients were associated with longer PFS than *MGMT*-unmethylated as previously reported [8, 19] ($p = 0.059$, Fig. 3). These parameters, however, did not show a statistically significant relationship with PFS (mean ADC value, $p = 0.667$; ADC entropy, $p = 0.797$, Fig. 3). We also did not find correlations between *MGMT* methylation status or these parameters and OS (not shown).

Discussion

The gold standard to detect the *MGMT* promoter methylation status in GBs is genetic analysis using surgical or biopsy specimens; however, such invasive procedures may cause severe complications. Moreover, sampling errors due to heterogeneous GB increase the risk of erroneous molecular profiling [6, 35]. Therefore, it would be helpful in deciding surgical strategy as well as overall treatment strategy in GBs, if the *MGMT* promoter methylation status can be evaluated noninvasively by preoperative imaging; the *MGMT*-methylated tumor could be subjected to resection together with implantation of BCNU wafers weighting the safety rather than radicality, and the *MGMT*-unmethylated tumor should perhaps be resected as much as safely with the possible risk of functional sequela. Indeed, several previous reports have suggested that BCNU wafer implantation followed by adjuvant radiotherapy and concomitant oral TMZ chemotherapy (the Stupp regimen) has an advantageous effect in *MGMT*-methylated GB patients compared with *MGMT*-unmethylated ones [27, 45], regardless of a high rate of adverse effects [2]. Preoperative prediction of *MGMT* methylation could also have an impact on the treatment and surgical strategy for noncodeleted lower-grade

Table 1 Molecular characteristics and qualitative imaging features of this cohort

Case no.	Age	Sex	IDH status	*MGMT* promoter methylation	WHO 2016 classification	Ring enhancement	Tumor location	Tumor laterality
1	57	Female	WT	U	Glioblastoma, IDH wild type	Other	Temporal	Left
2	58	Male	WT	M	Glioblastoma, IDH wild type	Ring	Callosal	Bilateral
3	28	Female	WT	U	Glioblastoma, IDH wild type	Ring	Nontemporal	Right
4	63	Female	WT	M	Glioblastoma, IDH wild type	Ring	Temporal	Left
5	57	Male	WT	U	Glioblastoma, IDH wild type	Other	Nontemporal	Left
6	67	Female	WT	M	Glioblastoma, IDH wild type	Ring	Temporal	Right
7	79	Male	WT	U	Glioblastoma, IDH wild type	Other	Temporal	Left
8	50	Female	WT	U	Glioblastoma, IDH wild type	Other	Nontemporal	Right
9	53	Male	WT	U	Glioblastoma, IDH wild type	Other	Temporal	Right
10	38	Male	WT	U	Glioblastoma, IDH wild type	Ring	Nontemporal	Left
11	54	Male	WT	U	Glioblastoma, IDH wild type	Other	Temporal	Right
12	62	Male	WT	U	Glioblastoma, IDH wild type	Ring	Temporal	Left
13	55	Male	WT	M	Glioblastoma, IDH wild type	Ring	Nontemporal	Left
14	49	Male	WT	U	Glioblastoma, IDH wild type	Other	Callosal	Bilateral
15	75	Male	WT	U	Glioblastoma, IDH wild type	Other	Nontemporal	Right
16	75	Male	WT	M	Glioblastoma, IDH wild type	Ring	Temporal	Left
17	76	Male	WT	M	Glioblastoma, IDH wild type	Ring	Temporal	Right
18	61	Male	WT	U	Glioblastoma, IDH wild type	Other	Temporal	Left
19	68	Female	WT	U	Glioblastoma, IDH wild type	Ring	Nontemporal	Left
20	80	Male	WT	U	Glioblastoma, IDH wild type	Ring	Temporal	Right
21	51	Male	WT	M	Glioblastoma, IDH wild type	Other	Temporal	Left
22	36	Male	WT	U	Glioblastoma, IDH wild type	Other	Temporal	Bilateral
23	79	Female	WT	M	Glioblastoma, IDH wild type	Ring	Callosal	Bilateral
24	62	Male	WT	U	Glioblastoma, IDH wild type	Ring	Nontemporal	Right
25	63	Female	WT	U	Glioblastoma, IDH wild type	Ring	Nontemporal	Left
26	53	Male	WT	M	Glioblastoma, IDH wild type	Ring	Callosal	Bilateral
27	61	Male	WT	U	Glioblastoma, IDH wild type	Ring	Nontemporal	Left
28	62	Female	Mut	M	Glioblastoma, IDH mutant	Ring	Temporal	Right
29	62	Female	WT	M	Glioblastoma, IDH wild type	Ring	Temporal	Left
30	79	Male	WT	U	Glioblastoma, IDH wild type	Ring	Temporal	Left
31	60	Female	WT	U	Glioblastoma, IDH wild type	Ring	Callosal	Bilateral
32	70	Male	WT	U	Glioblastoma, IDH wild type	Ring	Nontemporal	Right
33	67	Female	WT	M	Glioblastoma, IDH wild type	Other	Nontemporal	Bilateral
34	82	Male	WT	M	Glioblastoma, IDH wild type	Ring	Nontemporal	Right
35	73	Male	WT	U	Glioblastoma, IDH wild type	Ring	Temporal	Right
36	59	Male	WT	U	Glioblastoma, IDH wild type	Other	Nontemporal	Left
37	53	Male	WT	M	Glioblastoma, IDH wild type	Ring	Nontemporal	Left
38	85	Female	WT	U	Glioblastoma, IDH wild type	Ring	Nontemporal	Left
39	35	Female	WT	M	Glioblastoma, IDH wild type	Other	Nontemporal	Right
40	41	Male	WT	M	Glioblastoma, IDH wild type	Other	Temporal	Left
41	45	Male	WT	M	Glioblastoma, IDH wild type	Other	Nontemporal	Left
42	25	Female	WT	M	Glioblastoma, IDH wild type	Ring	Callosal	Bilateral
43	48	Male	WT	U	Glioblastoma, IDH wild type	Other	Callosal	Bilateral
44	77	Female	WT	M	Glioblastoma, IDH wild type	Ring	Nontemporal	Left
45	64	Female	WT	U	Glioblastoma, IDH wild type	Ring	Nontemporal	Left
46	53	Male	WT	M	Glioblastoma, IDH wild type	Ring	Temporal	Right
47	63	Male	WT	U	Glioblastoma, IDH wild type	Ring	Nontemporal	Right
48	74	Male	WT	M	Glioblastoma, IDH wild type	Ring	Nontemporal	Left

Mut, mutant; *WT*, wild type; *M*, methylated; *U*, unmethylated; *IDH*, isocitrate dehydrogenase; *MGMT*, O^6-methylguanine-DNA methyltransferase; *WHO*, World Health Organization

gliomas [39], because the interim analysis of the phase III trial in anaplastic gliomas lacking 1p/19q codeletion suggested that *MGMT* methylation is independently associated with patient survival with those tumors [46].

Prediction of methylation status of the *MGMT* gene in GBs by imaging is challenging. To date, several MRI features by visual assessment, including ring enhancement, tumor location, and laterality, have been reported to be associated with *MGMT* methylation status [7, 9, 10], but there is no consensus on these associations [15]. In the present study, we did not identify associations between qualitative imaging features and *MGMT* methylation status. Ring enhancement has been used as the most likely potential predictive marker for unmethylated

Table 2 Comparison of imaging parameters and *MGMT* promoter methylation status

	MGMT-methylated ($n = 21$)	*MGMT*-unmethylated ($n = 27$)	*p* value
Ring enhancement	Ring $n = 16$, other $n = 5$	Ring $n = 15$, other $n = 12$	0.138
Tumor location	Temporal $n = 9$, nontemporal $n = 8$, callosal $n = 4$	Temporal $n = 10$, nontemporal $n = 14$, callosal $n = 3$	0.577
Tumor laterality	Right $n = 6$, left $n = 10$, bilateral $n = 5$	Right $n = 10$, left $n = 13$, bilateral $n = 4$	0.682
Mean ADC value	1.191 ± 0.142	1.067 ± 0.120	*0.002*
ADC entropy	6.287 ± 0.272	5.972 ± 0.506	*0.013*
ADC skewness	0.704 ± 0.602	0.999 ± 1.755	0.465
ADC kurtosis	4.520 ± 2.349	4.612 ± 2.439	0.895

Italicized measures indicate measures that remained significant after false discovery rate (FDR) correction. Values are mean ± standard deviation

ADC, apparent diffusion coefficient; *MGMT*, O^6-methylguanine-DNA methyltransferase

MGMT promoter [7, 10]. In Drabycz's study, > 90% of *MGMT*-unmethylated groups were evaluated as ring enhanced, but we found that only 55.6% of *MGMT*-unmethylated groups were evaluated as the same. This result may be partially attributed to the difference in ring enhancement definitions (ring or nodular versus ring or other). Previous studies have demonstrated that *MGMT* promoter methylation correlated with the parietal and occipital lobes [10], the left hemisphere and temporal lobe [9], and subventricular zone [17] or was independent from tumor location [23]. In this study, tumor location, including tumor laterality, was not significantly associated with *MGMT* promoter methylation.

ADC also has been reported as a potential predictive marker for *MGMT* promoter methylation [5, 16, 17, 31, 34, 37, 44], but there is no expert consensus on this point. ADC indirectly reflects water proton movement. Greater cellularity results in lower ADC value, because most water motions occur in the extracellular space. Therefore, ADC has been used as an imaging marker of cellularity for various tumors [14, 41]. In the present study, texture analysis showed that the mean ADC value and ADC entropy were predictive of *MGMT* promoter methylation with sufficiently high sensitivity and specificity. Similar to our results, those of several previous reports have shown that ADC values were higher in *MGMT*-methylated tumors than in *MGMT*-unmethylated tumors [17, 31, 37, 44]. On the other hand, lower ADC values in *MGMT*-methylated GBs were reported [34], but this might have been because of the difference in cohorts (GBs only, not newly diagnosed bevacizumab-treated GBs). With regard to the association between ADC entropy and *MGMT* promoter methylation, our previous study supported this result [22]. In lower-grade gliomas, we have reported the association between tumor heterogeneity and *MGMT* promoter methylation. These two results indicate that there could be an association between tumor heterogeneity and *MGMT* promoter methylation in all types of glioma.

Several previous reports suggested that *MGMT*-methylated GBs might have more heterogeneous or lower cellularity according to the correlation between *MGMT* methylation and ADC value/CT attenuation [3, 31]. These suggestions supported our results. However, despite vigorous literature search, we could identify only one report on the pathomorphological relation between ADC value and *MGMT* promoter methylation [44]. Sunwoo et al. reported a negative relationship between the 5th percentile ADC value and the Ki-67 labeling index in GBs. In this report, Ki-67 IHC was used for the evaluation of tumor cell density, and elevated Ki-67 labeling index reflected increased cellularity (low ADC value) in *MGMT*-unmethylated GB. But the Ki-67 index is not representative of the entire tumor, because pathologists usually select the fields expressing the highest number of positive cells. Further histopathological investigation is needed to clarify the pathomorphological mechanism.

Our study also revealed that the mean ADC value and ADC entropy were negatively correlated with the *MGMT*-positive cell ratio in IHC analysis, which was almost the same result as that found in a previously described study [44]. Sunwoo et al. reported a positive relationship between the mean ADC value and the *MGMT* promoter methylation ratio semiquantitatively analyzed by using methylation-specific multiplex ligation-dependent probe amplification in GBs. We used IHC analysis to quantitatively evaluate the association between the imaging parameters and *MGMT* promoter methylation ratio because it was an easier and less expensive method.

Furthermore, our result did not find correlations between the mean ADC value or ADC entropy and PFS. These results were different from those of Sunwoo's report [44], but this might be attributed to heterogeneity of postoperative treatment in our case, which could affect clinical outcome data (MCNU or TMZ; RT 40 Gy or RT 60 Gy).

Finally, the main theme of this study was to identify imaging parameters to predict *MGMT* promoter methylation in GBs by using a commercially available software (Synapse

Table 3 Predictive values for *MGMT* promoter methylation by ADC parameters and the combination of these parameters

	PPV (%)	NPV (%)	Sensitivity (%)	Specificity (%)	*p* value
Mean ADC value	70.8 (17/24)	83.3 (20/24)	81.0 (17/21)	74.1 (20/27)	0.000
ADC entropy	68.2 (15/22)	76.9 (20/26)	71.4 (15/21)	74.1 (20/27)	0.002
Mean ADC value and ADC entropy	81.2 (13/16)	75 (24/32)	61.9 (13/21)	88.9 (24/27)	0.000

ADC, apparent diffusion coefficient; *PPV*, positive predictive value; *NPV*, negative predictive value

Vincent Fujifilm, Tokyo, Japan) and daily imaging data. Almost all previous texture analyses were performed by using in-house software. The widely used methodology is, therefore, suitable for routine clinical work. Currently, regardless of the time-consuming methods, machine-learning techniques are increasingly applied to predict *MGMT* methylation status from neuroimaging parameters in GBs [4, 21, 26]. These reports suggested that *MGMT* methylation status in GBs could be predicted with an accuracy of about 80% by using machine-learning algorithms. The sensitivity and specificity in our study may, therefore, be sufficiently high.

Study limitations

First, in the present study, the MR images were not acquired at the same magnetic field. At our institution, 1.5 T (before 2010) and 3 T (after 2011) MR imaging scanners were used. The difference in signal intensities on DW and ADC map images at different magnetic fields was not, however, important because molecular movement was independent from the magnetic field [1]. Of course, 3 T MR imaging was better than 1.5 T MR imaging in that the improvement of the signal-to-noise ratio made detection of tumor boundaries easier. However, manual ROI segmentation was not difficult even for 1.5 T MRI.

Second, this was a retrospective study with a relatively small sample size because patients without preoperative DW images (both $b = 0$ and 1000 s/mm^2) were excluded. It is recommended to validate our results using multivariate analyses in a larger cohort of patients prospectively.

Third, the current study had several limitations with regard to ROI application. ROI segmentation was determined by reference to the relatively higher signal on contrast-enhanced T1-weighted images, excluding cystic and necrotic regions. We evaluated only areas of enhancing tumor as previously reported because it was a more reproducible method [5, 17, 31, 34, 37, 44]. Despite the established method, possible bias due to manual drawing and visual positioning of ROIs was unavoidable. Then, in the current study, slice thickness on contrast-enhanced T1-weighted images was 5 mm. As slice thickness increases, the error in ROI delineation may increase because of partial volume effects [11]. Furthermore, ROI segmentation needed co-registration of contrast-enhanced T1-weighted images with ADC maps. The co-registration can even enhance these effects, if slices are not perfectly aligned between both image types. High-resolution 3D T1-weighted images (e.g., section thickness, 1 mm) would provide more accurate measurements.

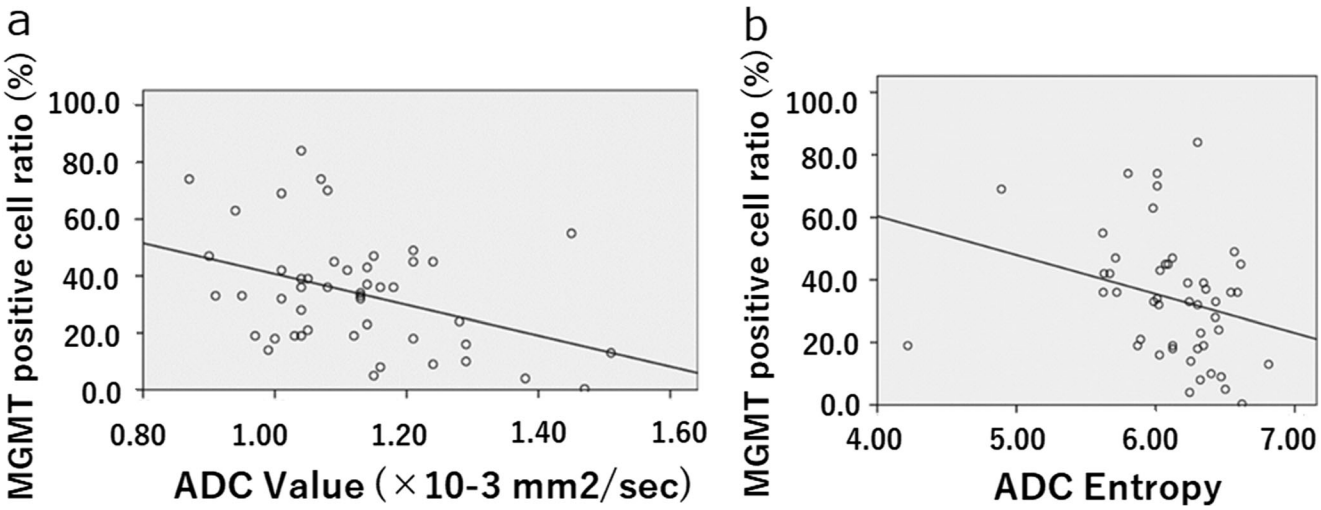

Fig. 2 Negative correlations between ADC parameters and *MGMT*-positive cell ratio in IHC. The Pearson linear regression plot revealed negative associations between ADC parameters and *MGMT*-positive cell ratio in IHC. **a** *MGMT*-positive cell ratio and mean ADC value; $R^2 = 0.153$, $p = 0.006$. **b** *MGMT*-positive cell ratio and ADC entropy; $R^2 = 0.78$, $p = 0.054$

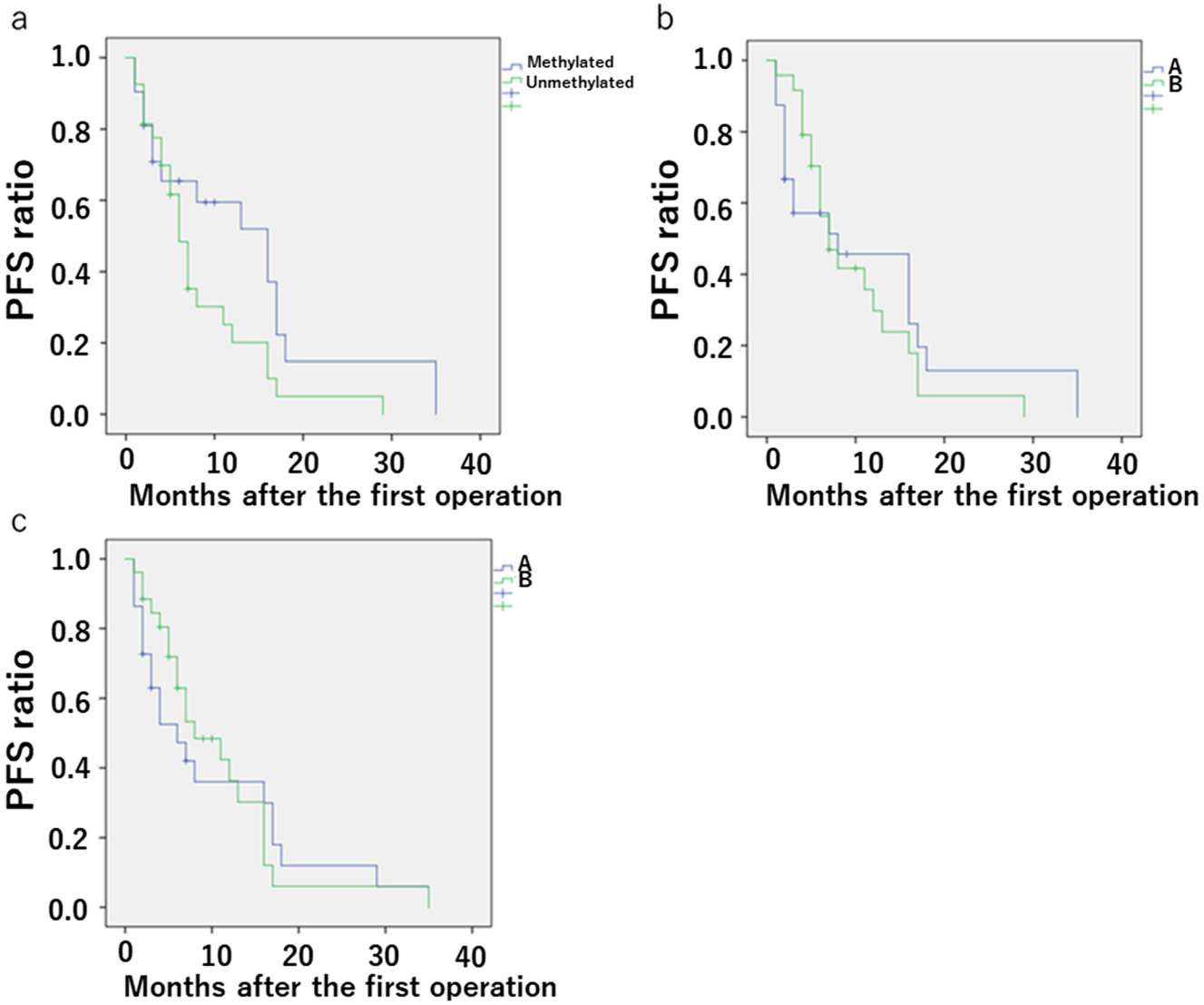

Fig. 3 Kaplan–Meier progression-free survival (PFS) curves based on the *MGMT* methylation status, mean ADC value, and ADC entropy in GB patients. **a** Time to tumor recurrence. *MGMT*-unmethylated patients showed earlier recurrence than *MGMT*-methylated patients ($p = 0.059$). **b** Time to tumor recurrence. "A," categorized by a mean ADC value ≥ 1.12; "B," categorized by a mean ADC value < 1.12. The mean ADC value did not show a statistically significant relationship with PFS ($p = 0.667$). **c** Time to tumor recurrence. "A," categorized by an ADC entropy ≥ 6.243; "B," categorized by ADC entropy < 6.243. The ADC entropy did not also show a statistically significant relationship with PFS ($p = 0.797$)

Finally, although the assessment consistency for qualitative analysis between the two observers (HS and TK) was good ($\kappa = 0.864$ (0.788–0.940)), interobserver bias still existed.

Conclusions

In conclusion, we used a commercially available software to demonstrate that the mean ADC value and ADC entropy could be used for predicting *MGMT* promoter methylation with sufficiently high PPV and specificity. These image parameters may be useful in designing personalized treatment preoperatively in GB patients.

Acknowledgements We greatly thank Ms. Naoko Tsuzaki at the Department of Neurosurgery, Keio University School of Medicine for technical assistance of laboratory works. The authors also greatly thank Dr. Takayuki Abe at the Center for Clinical Research, Department of Preventive Medicine and Public Health, Keio University School of Medicine for statistical advice.

Compliance with ethical standards

Conflict of interest The authors declare that they have no conflict of interest.

Ethical approval This study was approved by the Institutional Review Board of Keio University. All procedures performed in studies involving human participants were in accordance with the ethical standards of the institutional and/or national research committee and with the 1964 Helsinki declaration and its later amendments or comparable ethical standards.

Informed consent Informed consent was obtained from all individual participants included in the study.

Publisher's Note Springer Nature remains neutral with regard to jurisdictional claims in published maps and institutional affiliations.

References

1. Alvarez-Linera J (2008) 3T MRI: advances in brain imaging. Eur J Radiol 67:415–426. https://doi.org/10.1016/j.ejrad.2008.02.045
2. Ashby LS, Smith KA, Stea B (2016) Gliadel wafer implantation combined with standard radiotherapy and concurrent followed by adjuvant temozolomide for treatment of newly diagnosed high-grade glioma: a systematic literature review. World J Surg Oncol 14:225. https://doi.org/10.1186/s12957-016-0975-5
3. Barajas RF Jr, Hodgson JG, Chang JS, Vandenberg SR, Yeh RF, Parsa AT, McDermott MW, Berger MS, Dillon WP, Cha S (2010) Glioblastoma multiforme regional genetic and cellular expression patterns: influence on anatomic and physiologic MR imaging. Radiology 254:564–576. https://doi.org/10.1148/radiol.09090663
4. Chang P, Grinband J et al (2018) Deep-learning convolutional neural networks accurately classify genetic mutations in gliomas. AJNR Am J Neuroradiol 39:1201–1207. https://doi.org/10.3174/ajnr.A5667
5. Choi YS, Ahn SS, Kim DW, Chang JH, Kang SG, Kim EH, Kim SH, Rim TH, Lee SK (2016) Incremental prognostic value of ADC histogram analysis over MGMT promoter methylation status in patients with glioblastoma. Radiology 281:175–184. https://doi.org/10.1148/radiol.2016151913
6. Coons SW, Johnson PC, Scheithauer BW, Yates AJ, Pearl DK (1997) Improving diagnostic accuracy and interobserver concordance in the classification and grading of primary gliomas. Cancer 79:1381–1393
7. Drabycz S, Roldan G, de Robles P, Adler D, McIntyre JB, Magliocco AM, Cairncross JG, Mitchell JR (2010) An analysis of image texture, tumor location, and MGMT promoter methylation in glioblastoma using magnetic resonance imaging. NeuroImage 49:1398–1405. https://doi.org/10.1016/j.neuroimage.2009.09.049
8. Dunn J, Baborie A, Alam F, Joyce K, Moxham M, Sibson R, Crooks D, Husband D, Shenoy A, Brodbelt A, Wong H, Liloglou T, Haylock B, Walker C (2009) Extent of MGMT promoter methylation correlates with outcome in glioblastomas given temozolomide and radiotherapy. Br J Cancer 101:124–131. https://doi.org/10.1038/sj.bjc.6605127
9. Ellingson BM, Cloughesy TF, Pope WB, Zaw TM, Phillips H, Lalezari S, Nghiemphu PL, Ibrahim H, Naeini KM, Harris RJ, Lai A (2012) Anatomic localization of O6-methylguanine DNA methyltransferase (MGMT) promoter methylated and unmethylated tumors: a radiographic study in 358 de novo human glioblastomas. NeuroImage 59:908–916. https://doi.org/10.1016/j.neuroimage.2011.09.076
10. Eoli M, Menghi F, Bruzzone MG, De Simone T, Valletta L, Pollo B, Bissola L, Silvani A, Bianchessi D, D'Incerti L, Filippini G, Broggi G, Boiardi A, Finocchiaro G (2007) Methylation of O6-methylguanine DNA methyltransferase and loss of heterozygosity on 19q and/or 17p are overlapping features of secondary glioblastomas with prolonged survival. Clin Cancer Res 13:2606–2613. https://doi.org/10.1158/1078-0432.CCR-06-2184
11. Firbank MJ, Coulthard A, Harrison RM, Williams ED (1999) Partial volume effects in MRI studies of multiple sclerosis. Magn Reson Imaging 17:593–601
12. Fukushima T, Takeshima H, Kataoka H (2009) Anti-glioma therapy with temozolomide and status of the DNA-repair gene MGMT. Anticancer Res 29:4845–4854
13. Glickman ME, Rao SR, Schultz MR (2014) False discovery rate control is a recommended alternative to Bonferroni-type adjustments in health studies. J Clin Epidemiol 67:850–857. https://doi.org/10.1016/j.jclinepi.2014.03.012
14. Guo AC, Cummings TJ, Dash RC, Provenzale JM (2002) Lymphomas and high-grade astrocytomas: comparison of water diffusibility and histologic characteristics. Radiology 224:177–183. https://doi.org/10.1148/radiol.2241010637
15. Gupta A, Omuro AM, Shah AD, Graber JJ, Shi W, Zhang Z, Young RJ (2012) Continuing the search for MR imaging biomarkers for MGMT promoter methylation status: conventional and perfusion MRI revisited. Neuroradiology 54:641–643. https://doi.org/10.1007/s00234-011-0970-z
16. Gupta A, Prager A, Young RJ, Shi W, Omuro AM, Graber JJ (2013) Diffusion-weighted MR imaging and MGMT methylation status in glioblastoma: a reappraisal of the role of preoperative quantitative ADC measurements. AJNR Am J Neuroradiol 34:E10–E11. https://doi.org/10.3174/ajnr.A3467
17. Han Y, Yan LF, Wang XB, Sun YZ, Zhang X, Liu ZC, Nan HY, Hu YC, Yang Y, Zhang J, Yu Y, Sun Q, Tian Q, Hu B, Xiao G, Wang W, Cui GB (2018) Structural and advanced imaging in predicting MGMT promoter methylation of primary glioblastoma: a region of interest based analysis. BMC Cancer 18:215. https://doi.org/10.1186/s12885-018-4114-2
18. Hegi ME, Diserens AC, Godard S, Dietrich PY, Regli L, Ostermann S, Otten P, Van Melle G, de Tribolet N, Stupp R (2004) Clinical trial substantiates the predictive value of O-6-methylguanine-DNA methyltransferase promoter methylation in glioblastoma patients treated with temozolomide. Clin Cancer Res 10:1871–1874
19. Hegi ME, Diserens AC, Gorlia T, Hamou MF, de Tribolet N, Weller M, Kros JM, Hainfellner JA, Mason W, Mariani L, Bromberg JE, Hau P, Mirimanoff RO, Cairncross JG, Janzer RC, Stupp R (2005) MGMT gene silencing and benefit from temozolomide in glioblastoma. N Engl J Med 352:997–1003. https://doi.org/10.1056/NEJMoa043331
20. Hsu CY, Lin SC, Ho HL, Chang-Chien YC, Hsu SP, Yen YS, Chen MH, Guo WY, Ho DM (2013) Exclusion of histiocytes/endothelial cells and using endothelial cells as internal reference are crucial for interpretation of MGMT immunohistochemistry in glioblastoma. Am J Surg Pathol 37:264–271. https://doi.org/10.1097/PAS.0b013e318267b061
21. Kanas VG, Zacharaki EI, Thomas GA, Zinn PO, Megalooikonomou V, Colen RR (2017) Learning MRI-based classification models for MGMT methylation status prediction in glioblastoma. Comput Methods Prog Biomed 140:249–257. https://doi.org/10.1016/j.cmpb.2016.12.018
22. Kanazawa T, Fujiwara H, Takahashi H, Nishiyama Y, Hirose Y, Tanaka S, Yoshida K, Sasaki H (2018) Imaging scoring systems for preoperative molecular diagnoses of lower-grade gliomas. Neurosurg Rev. https://doi.org/10.1007/s10143-018-0981-x
23. Kickingereder P, Bonekamp D, Nowosielski M, Kratz A, Sill M, Burth S, Wick A, Eidel O, Schlemmer HP, Radbruch A, Debus J, Herold-Mende C, Unterberg A, Jones D, Pfister S, Wick W, von Deimling A, Bendszus M, Capper D (2016) Radiogenomics of glioblastoma: machine learning-based classification of molecular characteristics by using multiparametric and multiregional MR

imaging features. Radiology 281:907–918. https://doi.org/10.1148/radiol.2016161382
24. Kleihues P, Burger PC, Scheithauer BW (1993) Histological typing of tumors of the central nervous system, 2nd edn. Springer, Berlin
25. Kleihues P, Cavanee W (2000) Pathology and genetics of tumors of the nervous system. International Agency for Research on Cancer Press, Lyon
26. Korfiatis P, Kline TL, Coufalova L, Lachance DH, Parney IF, Carter RE, Buckner JC, Erickson BJ (2016) MRI texture features as biomarkers to predict MGMT methylation status in glioblastomas. Med Phys 43:2835–2844. https://doi.org/10.1118/1.4948668
27. Lechapt-Zalcman E, Levallet G, Dugue AE, Vital A, Diebold MD, Menei P, Colin P, Peruzzy P, Emery E, Bernaudin M, Chapon F, Guillamo JS (2012) O(6)-methylguanine-DNA methyltransferase (MGMT) promoter methylation and low MGMT-encoded protein expression as prognostic markers in glioblastoma patients treated with biodegradable carmustine wafer implants after initial surgery followed by radiotherapy with concomitant and adjuvant temozolomide. Cancer 118:4545–4554. https://doi.org/10.1002/cncr.27441
28. Louis DN, Ohgaki H, Wiestler OD, Cavenee WK (2007) WHO classification of tumours of the central nervous system, 4th edn. International Agency for Research on Cancer, Lyon
29. Louis DN, Ohgaki H, Wiestler OD, Cavenee WK, Ellison DW, Figarella-Branger D, Perry A, Reifenberger G, von Deimling A (2016) WHO classification of tumours of the central nervous system. In: Revised 4th edn. International Agency for Research on Cancer, Lyon
30. Miwa T, Hirose Y, Sasaki H, Ikeda E, Yoshida K, Kawase T (2009) Genetic characterization of adult infratentorial gliomas. J Neuro-Oncol 91:251–255. https://doi.org/10.1007/s11060-008-9714-2
31. Moon WJ, Choi JW, Roh HG, Lim SD, Koh YC (2012) Imaging parameters of high grade gliomas in relation to the MGMT promoter methylation status: the CT, diffusion tensor imaging, and perfusion MR imaging. Neuroradiology 54:555–563. https://doi.org/10.1007/s00234-011-0947-y
32. Omuro A, DeAngelis LM (2013) Glioblastoma and other malignant gliomas: a clinical review. Jama 310:1842–1850. https://doi.org/10.1001/jama.2013.280319
33. Ostrom QT, Gittleman H, Fulop J, Liu M, Blanda R, Kromer C, Wolinsky Y, Kruchko C, Barnholtz-Sloan JS (2015) CBTRUS statistical report: primary brain and central nervous system tumors diagnosed in the United States in 2008-2012. Neuro-Oncology 17(Suppl 4):iv1–iv62. https://doi.org/10.1093/neuonc/nov189
34. Pope WB, Lai A, Mehta R, Kim HJ, Qiao J, Young JR, Xue X, Goldin J, Brown MS, Nghiemphu PL, Tran A, Cloughesy TF (2011) Apparent diffusion coefficient histogram analysis stratifies progression-free survival in newly diagnosed bevacizumab-treated glioblastoma. AJNR Am J Neuroradiol 32:882–889. https://doi.org/10.3174/ajnr.A2385
35. Prayson RA, Agamanolis DP, Cohen ML, Estes ML, Kleinschmidt-DeMasters BK, Abdul-Karim F, McClure SP, Sebek BA, Vinay R (2000) Interobserver reproducibility among neuropathologists and surgical pathologists in fibrillary astrocytoma grading. J Neurol Sci 175:33–39
36. Riemenschneider MJ, Hegi ME, Reifenberger G (2010) MGMT promoter methylation in malignant gliomas. Target Oncol 5:161–165. https://doi.org/10.1007/s11523-010-0153-6
37. Romano A, Calabria LF, Tavanti F, Minniti G, Rossi-Espagnet MC, Coppola V, Pugliese S, Guida D, Francione G, Colonnese C, Fantozzi LM, Bozzao A (2013) Apparent diffusion coefficient obtained by magnetic resonance imaging as a prognostic marker in glioblastomas: correlation with MGMT promoter methylation status. Eur Radiol 23:513–520. https://doi.org/10.1007/s00330-012-2601-4
38. Ronning PA, Helseth E, Meling TR, Johannesen TB (2012) A population-based study on the effect of temozolomide in the treatment of glioblastoma multiforme. Neuro-Oncology 14:1178–1184. https://doi.org/10.1093/neuonc/nos153
39. Sasaki H, Hirose Y, Yazaki T, Kitamura Y, Katayama M, Kimura T, Fujiwara H, Toda M, Ohira T, Yoshida K (2015) Upfront chemotherapy and subsequent resection for molecularly defined gliomas. J Neuro-Oncol 124:127–135. https://doi.org/10.1007/s11060-015-1817-y
40. Sasaki H, Zlatescu MC, Betensky RA, Ino Y, Cairncross JG, Louis DN (2001) PTEN is a target of chromosome 10q loss in anaplastic oligodendrogliomas and PTEN alterations are associated with poor prognosis. Am J Pathol 159:359–367. https://doi.org/10.1016/s0002-9440(10)61702-6
41. Squillaci E, Manenti G, Cova M, Di Roma M, Miano R, Palmieri G, Simonetti G (2004) Correlation of diffusion-weighted MR imaging with cellularity of renal tumours. Anticancer Res 24:4175–4179
42. Stupp R, Mason WP, van den Bent MJ, Weller M, Fisher B, Taphoorn MJ, Belanger K, Brandes AA, Marosi C, Bogdahn U, Curschmann J, Janzer RC, Ludwin SK, Gorlia T, Allgeier A, Lacombe D, Cairncross JG, Eisenhauer E, Mirimanoff RO (2005) Radiotherapy plus concomitant and adjuvant temozolomide for glioblastoma. N Engl J Med 352:987–996. https://doi.org/10.1056/NEJMoa043330
43. Stupp R, Taillibert S, Kanner AA, Kesari S, Steinberg DM, Toms SA, Taylor LP, Lieberman F, Silvani A, Fink KL, Barnett GH, Zhu JJ, Henson JW, Engelhard HH, Chen TC, Tran DD, Sroubek J, Tran ND, Hottinger AF, Landolfi J, Desai R, Caroli M, Kew Y, Honnorat J, Idbaih A, Kirson ED, Weinberg U, Palti Y, Hegi ME, Ram Z (2015) Maintenance therapy with tumor-treating fields plus temozolomide vs temozolomide alone for glioblastoma: a randomized clinical trial. Jama 314:2535–2543. https://doi.org/10.1001/jama.2015.16669
44. Sunwoo L, Choi SH, Park CK, Kim JW, Yi KS, Lee WJ, Yoon TJ, Song SW, Kim JE, Kim JY, Kim TM, Lee SH, Kim JH, Sohn CH, Park SH, Kim IH, Chang KH (2013) Correlation of apparent diffusion coefficient values measured by diffusion MRI and MGMT promoter methylation semiquantitatively analyzed with MS-MLPA in patients with glioblastoma multiforme. J Magn Reson Imaging 37:351–358. https://doi.org/10.1002/jmri.23838
45. Urbschat S, Sippl C, Engelhardt J, Kammers K, Oertel J, Ketter R (2017) Importance of biomarkers in glioblastomas patients receiving local BCNU wafer chemotherapy. Mol Cytogenet 10:16. https://doi.org/10.1186/s13039-017-0317-5
46. van den Bent MJ, Baumert B, Erridge SC, Vogelbaum MA, Nowak AK, Sanson M, Brandes AA, Clement PM, Baurain JF, Mason WP, Wheeler H, Chinot OL, Gill S, Griffin M, Brachman DG, Taal W, Ruda R, Weller M, McBain C, Reijneveld J, Enting RH, Weber DC, Lesimple T, Clenton S, Gijtenbeek A, Pascoe S, Herrlinger U, Hau P, Dhermain F, van Heuvel I, Stupp R, Aldape K, Jenkins RB, Dubbink HJ, Dinjens WNM, Wesseling P, Nuyens S, Golfinopoulos V, Gorlia T, Wick W, Kros JM (2017) Interim results from the CATNON trial (EORTC study 26053-22054) of treatment with concurrent and adjuvant temozolomide for 1p/19q non-co-deleted anaplastic glioma: a phase 3, randomised, open-label intergroup study. Lancet 390:1645–1653. https://doi.org/10.1016/s0140-6736(17)31442-3
47. Weller M, Stupp R, Reifenberger G, Brandes AA, van den Bent MJ, Wick W, Hegi ME (2010) MGMT promoter methylation in malignant gliomas: ready for personalized medicine? Nat Rev Neurol 6:39–51. https://doi.org/10.1038/nrneurol.2009.197